JOURNAL OF PROPULSION AND POWER
Vol. 18, No. 2, March–April 2002

Impeller Blade Unsteady Aerodynamic Response to Vaned Diffuser Potential Fields

Dana Gottfried* and Sanford Fleeter†
Purdue University, West Lafayette, Indiana 47907

To predict the unsteady aerodynamic response of centrifugal compressor impeller blades to the potential field generated by the downstream vaned diffuser, a small perturbation model is developed that considers the number of impeller blades and diffuser vanes, the impeller blade backsweep angle, the impeller rotational speed, and the mass flow rate. The unsteady flow is analyzed in the impeller exit region and the vaneless diffuser space between the impeller and the diffuser leading edge radius, where the unsteady flow generated by the diffuser vane potential field is most significant. The unsteady flow perturbations are superimposed on an irrotational two-dimensional steady flow model, resulting in an analysis that is consistent with the small perturbation velocity potential equation. This model is then applied to a representative modern high speed impeller-vaned diffuser configuration.

Nomenclature

A	=	speed of sound
A_{0i}	=	stagnation speed of sound at inflow boundary
$\boldsymbol{G}$	=	impeller blade spacing vector
k	=	reduced frequency
k_d^m	=	tangential wave number at inlet boundary
k_θ^m	=	tangential wave number for continuous analytic solution
M_r	=	V_r/A
M_θ	=	V_θ/A
m	=	mode number
P_{oh}	=	stagnation pressure at the inflow boundary
p	=	perturbation pressure
r, θ, t	=	cylindrical coordinate directions and time in rotating impeller frame
r_i	=	grid inlet radius
r_t	=	impeller tip radius
r_v	=	radius of diffuser vane leading edges (radius of grid exit)
T_{oh}	=	stagnation temperature at the inflow boundary
$\boldsymbol{V}$	=	velocity in the stationary frame of reference
V_r	=	radial velocity
$\boldsymbol{V}_{\text{rel}}$	=	velocity in the rotating impeller frame
V_θ	=	tangential velocity in the stationary frame
$V_{\theta\,\text{rel}}$	=	tangential velocity in the rotating frame
$\boldsymbol{v}$	=	perturbation velocity
α	=	impeller blade angle with respect to radial
α_t	=	impeller blade angle at impeller exit
Γ^2	=	$1 - M_r^2$
ΔC_p	=	pressure coefficient differential across the impeller blade, $\Delta p/(\frac{1}{2}\rho_{oi} A_{oh}^2)$
ρ	=	perturbation density
ρ_{0i}	=	stagnation density at inflow boundary
σ	=	interblade phase angle
ϕ	=	perturbation velocity potential
ϕ_i	=	imposed potential disturbance at outflow
Ω	=	impeller rotational speed

Received 26 February 2001; revision received 19 July 2001; accepted for publication 13 August 2001.

*Postdoctoral Researcher, School of Mechanical Engineering. Member AIAA.

†McAllister Distinguished Professor, School of Mechanical Engineering; fleeter@ecn.purdue.edu. Fellow AIAA.

Introduction

THE trend in modern engines is toward decreased blade row spacing in engines that are more compact and lighter weight, thereby producing considerable savings in fuel consumption. However, as blade row spacing decreases, potential-flow-generated forcing functions become more important with regard to blade vibration problems. Thus, there is an increasing need for design tools that predict potential field effects on closely spaced blade row unsteady aerodynamics.

Experimentally, potential effects from downstream blade rows, both axial and radial, produce significant unsteadiness on upstream components when the spacing is small. Dring et al.[1] have shown that potential effects from a downstream axial flow turbine rotor cause significant unsteadiness on the aft portion of upstream stators, with the rotors 15% of the axial chord aft of the vanes. Iino and Kasai[2] have shown in their experimental study that potential effects from downstream diffuser vanes cause significant pressure fluctuations on impeller blades, with the vane inlet to impeller exit radius ratio being 1.03.

Whitehead[3] was the first to develop a potential flow theory to predict the unsteady aerodynamics of a flat plate axial cascade executing harmonic oscillations or subject to a vortical gust. Bryan and Fleeter[4] developed a radial cascade unsteady aerodynamic model by using a conformal transformation and a radial wake model in conjunction with a flat plate axial cascade analysis. Caruthers and Kurosaka[5] developed a small perturbation analysis to predict the unsteady aerodynamic force on impeller blades generated by the diffuser vane potential field, with the unsteady perturbations superimposed on a one-dimensional steady flow. This one-dimensional steady flow has a constant Mach number through the impeller blade passage, thereby capturing some features of the jet-wake effect found in actual impellers, that is, the jet in the impeller passage has been found experimentally to have a nearly constant Mach number. However, one-dimensional steady flow through a rotating impeller is not consistent with the small perturbation velocity potential equation, which requires the steady flow to be irrotational.

This research is directed at developing a valid model to predict the unsteady aerodynamic response of impeller blades to the potential field generated by the downstream vaned diffuser. This is accomplished by significantly extending the small perturbation modeling, initiated by Caruthers and Kurosaka,[5] which analyzes the unsteady flow in the impeller exit region and the vaneless space between the impeller and the diffuser leading edge radius, where the unsteadiness produced by the diffuser vanes is most pronounced. In particular, in

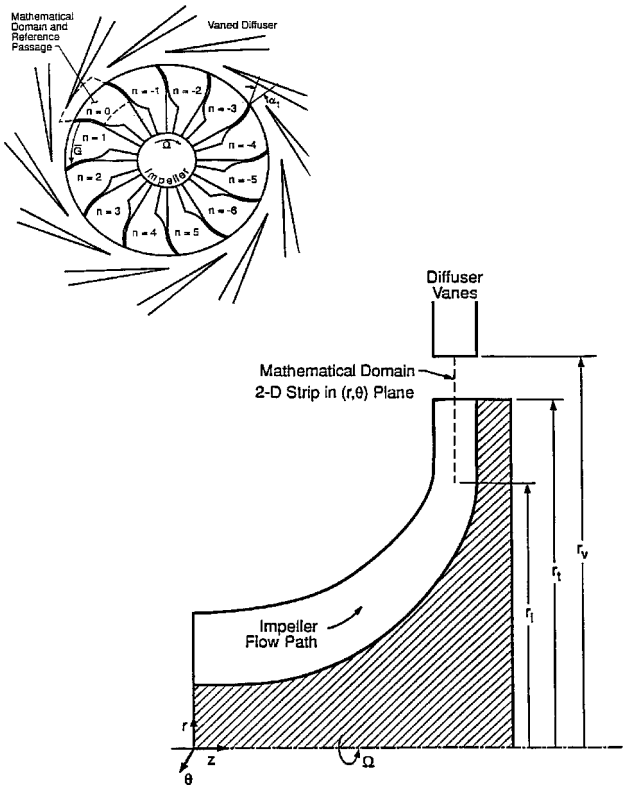

Fig. 1 Centrifugal compressor mathematical domain.

this paper, the unsteady flow perturbations are superimposed on an irrotational two-dimensional steady flow model, resulting in an analysis that is consistent with the small perturbation velocity potential equation. The mathematical domain is a two-dimensional strip in the impeller exit region (Fig. 1). Restricting the domain to the impeller tip region is mathematically convenient because, in this region, the flowfield is approximately radial. This means the flow equations can be written in cylindrical coordinates, a considerable simplification over writing them in meridional coordinates. Only one blade passage is considered because the flow is periodic in the tangential direction. With the interblade phase angle σ, this linear model is general enough to handle any ratio of impeller blade count to diffuser blade count. The blade is required to be radially oriented at the inflow boundary so that the inlet boundary condition can be properly applied.

Flow Equations

A small perturbation model is developed, with the unsteadiness assumed to be a small perturbation from the steady flow. Thus, each flow variable is decomposed into a time-independent part of order ε^0 and a time-dependent part of order ε^1, where $\varepsilon \ll 1$. When the notation of Verdon[6] is adopted, quantities with a tilde are time-dependent quantities, upper case quantities are zeroth order $\mathcal{O}(1)$, and lower case quantities are first order $\mathcal{O}(\varepsilon)$. The flowfield equations are expressed in dimensionless form. Lengths are scaled by the impeller tip radius r_t, time with the ratio of the impeller tip radius to the upstream stagnation sound speed, density with the upstream stagnation density, and temperature with the upstream stagnation temperature.

Conservation of mass and momentum in the radial and tangential directions and energy in the rotating impeller reference frame are

$$\frac{\partial \tilde{\bar{\rho}}}{\partial t} + \frac{\partial \tilde{\bar{\rho}} \tilde{V}_r}{\partial r} + \frac{1}{r}\frac{\partial \tilde{\bar{\rho}} \tilde{V}_{\theta\,\mathrm{rel}}}{\partial \theta} + \frac{\tilde{\bar{\rho}} \tilde{V}_r}{r} = 0 \tag{1}$$

$$\tilde{\bar{\rho}}\left(\frac{\partial \tilde{V}_r}{\partial t} + \tilde{V}_r\frac{\partial \tilde{V}_r}{\partial r} + \frac{\tilde{V}_{\theta\,\mathrm{rel}}}{r}\frac{\partial \tilde{V}_r}{\partial \theta} - \frac{\tilde{V}_\theta}{r}\right) = -\frac{\partial \tilde{P}}{\partial r} \tag{2a}$$

$$\tilde{\bar{\rho}}\left(\frac{\partial \tilde{V}_\theta}{\partial t} + \tilde{V}_r\frac{\partial \tilde{V}_\theta}{\partial r} + \frac{\tilde{V}_\theta \tilde{V}_r}{r} + \frac{\tilde{V}_{\theta\,\mathrm{rel}}}{r}\frac{\partial \tilde{V}_\theta}{\partial \theta}\right) = -\frac{1}{r}\frac{\partial \tilde{P}}{\partial \theta} \tag{2b}$$

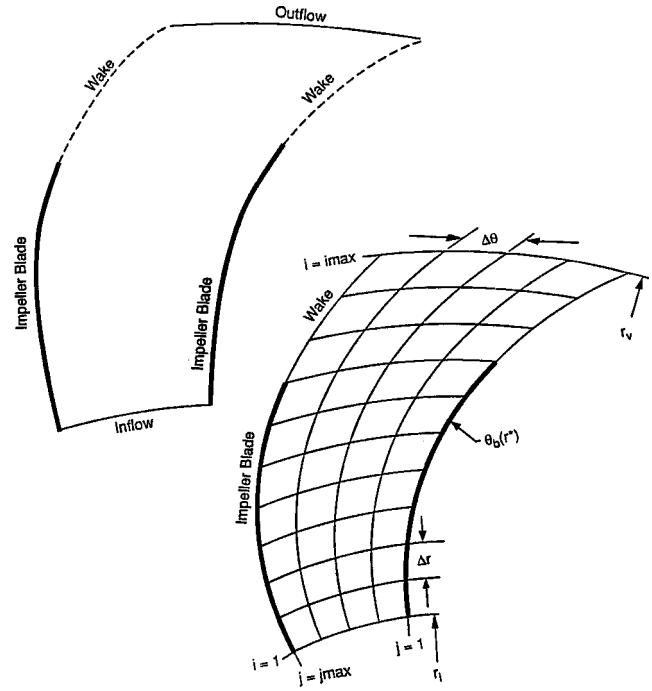

Fig. 2 Flowfield boundaries and grid.

$$\tilde{\bar{\rho}}\frac{\partial \tilde{H}_o}{\partial t} + \tilde{\bar{\rho}}\tilde{V}_r\frac{\partial \tilde{H}_o}{\partial r} + \tilde{\bar{\rho}}\frac{\tilde{V}_{\theta\,\mathrm{rel}}}{r}\frac{\partial \tilde{H}_o}{\partial \theta} - \frac{\partial \tilde{P}}{\partial t} + \Omega\frac{\partial \tilde{P}}{\partial \theta} = 0 \tag{3}$$

where $\tilde{V}_{\theta\,\mathrm{rel}} = \tilde{V}_\theta - r\Omega$ is the tangential velocity in the rotating frame.

For isentropic flow of a perfect gas, the thermodynamic relations are

$$\tilde{P} = (1/\gamma)\tilde{\bar{\rho}} \qquad \tilde{H} = [1/(\gamma-1)]\tilde{T} \qquad \gamma\tilde{P} = \tilde{\bar{\rho}}^{\gamma}$$

$$\tilde{A}^2 = \gamma\tilde{P}/\tilde{\bar{\rho}} \tag{4}$$

There are four boundary conditions in the mathematical domain (Fig. 2). The flow must be tangent to the surface of the impeller blades to impose a solid wall condition:

$$\tilde{V}\cdot\hat{n}|_{\mathrm{blade}} = 0 \tag{5}$$

The pressure and normal velocity are continuous across the wake line, that is, the wakes are lines across which the tangential velocity may be discontinuous:

$$[[\tilde{P}]] = 0 \tag{6}$$

$$[[\tilde{V}]]\cdot\hat{n} = 0 \tag{7}$$

where [[ ]] refers to the difference in a flow quantity across the inviscid wake.

Steady Flow Model

The steady flow through the impeller is modeled as an irrotational two-dimensional flow, with one-dimensional steady flow also considered for comparison. The one-dimensional flow model solves the steady flow equations with the gradients in the tangential direction neglected. Integrating the steady mass conservation equation yields $\bar{\rho}V_r r = \text{const}$. Combining the steady conservation of tangential momentum and energy equations, the rothalpy equation is derived, $H_0 - r\Omega V_\theta = \text{const}$. For one-dimensional flow, the boundary condition of no flow through the blade reduces to $V_{\theta\,\mathrm{rel}} = V_r\tan(\alpha)$, where α is the impeller blade angle. Because there are no tangential gradients, this blade boundary condition equation is valid throughout the impeller passage. For flow in the vaneless space, conservation of angular momentum, $r(V_{\theta\,\mathrm{rel}} + r\Omega) = \text{const}$, applies. The steady

flow is calculated at the nodes of the computational grid, beginning at the inflow boundary and marching radially to the outflow boundary. At each tangential grid line, an iteration procedure is utilized that uses rothalpy, conservation of mass, and the thermodynamic relations.

The one-dimensional steady velocity field is rotational in the stationary reference frame. This is seen by noting that the curl of the velocity for one-dimensional flow is zero only if $r(V_{\theta\,\mathrm{rel}} + r\Omega) = \text{const}$. However, this is not true in the impeller passage because the blades are imparting angular momentum to the fluid.

The two-dimensional steady flow is calculated using the analysis of McFarland.[7] This analysis uses a panel method formulation to solve the inviscid irrotational compressible blade-to-blade flow equations on a surface of revolution. The exit flow angle is determined as part of the solution by using the Kutta condition to set the circulation around the airfoil. It assumes that the flow is irrotational and inviscid and solves the steady conservation of mass and irrotationality equations. Density gradients are permitted in the streamwise direction only. This two-dimensional steady flow model assumes that the impeller blades have finite thickness. However, the unsteady model assumes that the impeller blades have zero thickness, being represented by the blade mean lines. Therefore, the steady flow quantities along the blade surface are extrapolated to the mean line of the blade such that the velocity is tangent to the mean line. To reduce the error caused by the extrapolation, the blade thickness for this two-dimensional steady flow solver is made as small as possible.

Unsteady Flow Model

The first-order perturbation quantities are harmonic in time with their periodicity expressed by the interblade phase angle $\sigma = 2\pi$ number of diffuser vanes/number of impeller blades (NV/NB). Note that with the interblade phase angle σ, this linear model is general enough to handle any ratio of impeller blade count to diffuser blade count. Thus, for example, the perturbation pressure is

$$\tilde{p}(\boldsymbol{r}, t)\exp(in\sigma) = \mathrm{Re}\{p(\boldsymbol{r} + n\boldsymbol{G})\exp(ikt)\} \tag{8}$$

where p is the complex perturbation pressure amplitude, n indicates the number of blade passages away from the reference blade passage, (Fig. 1), $\boldsymbol{G}$ is a vector in the tangential direction with magnitude 2π/NB, and $k = NV(\Omega r_t / A_{0i})$ is the nondimensional frequency of the imposed disturbance, the reduced frequency.

The unsteady perturbation velocity is assumed to be irrotational. Thus, the perturbation velocity $\boldsymbol{v}$ is expressed in terms of the perturbation velocity potential, $\boldsymbol{v} = \nabla\phi$. The perturbation velocity potential equation is derived by substituting the flow variable perturbation expansions into the thermodynamic relations and the conservation of mass and momentum equations, and retaining only the first-order terms. Substituting the perturbation expansions into the third equation of Eq. (4), expanding by the binomial theorem, retaining only first-order terms, and using the steady form of the speed of sound equation yields the perturbation equation of state $p = \rho A^2$.

Substituting the variable expansions into the continuity equation [Eq. (1)] and retaining only first-order terms, the perturbation mass conservation equation in the impeller reference frame is

$$\bar{\rho}\frac{\bar{\mathrm{D}}(\rho/\bar{\rho})}{\mathrm{D}t} + \nabla\cdot(\bar{\rho}\nabla\phi) = 0 \tag{9}$$

where $\bar{\mathrm{D}}/\mathrm{D}t = ik + \boldsymbol{V}_{\mathrm{rel}}\cdot\nabla$ and $\boldsymbol{V}_{\mathrm{rel}}$ is the steady velocity in the impeller reference frame.

Similarly, substituting the flow variable expansions into Eq. (2), retaining only first-order terms, and using Eq. (9) to eliminate terms, the perturbation momentum equation in the rotating frame of reference is

$$\frac{\bar{\mathrm{D}}\nabla\phi}{\mathrm{D}t} + (\nabla\phi\cdot\nabla)\boldsymbol{V} + \nabla\left(\frac{p}{\bar{\rho}}\right) = 0 \tag{10}$$

If the steady velocity field in the stationary reference frame is irrotational, that is, $\nabla\times\boldsymbol{V} = 0$, this equation can be further simplified to

$$p = -\bar{\rho}\frac{\bar{\mathrm{D}}\phi}{\mathrm{D}t} \tag{11}$$

Combining Eqs. (9) and (11) and $p = \rho A^2$ gives the perturbation velocity potential equation:

$$\bar{\rho}\frac{\bar{\mathrm{D}}}{\mathrm{D}t}\left(\frac{1}{A^2}\frac{\bar{\mathrm{D}}\phi}{\mathrm{D}t}\right) - \nabla\cdot(\bar{\rho}\nabla\phi) = 0 \tag{12}$$

This is a linear scalar differential equation in terms of only the perturbation velocity potential ϕ. This equation describes the unsteady perturbation flow in the centrifugal compressor generated by the potential field of the downstream vaned diffuser.

Boundary Conditions

The blade surface and wake boundary conditions are determined by substituting the variable expansions into the boundary conditions of Eqs. (5–7) and retaining only first-order terms. The blade surface boundary condition is

$$\left.\frac{\partial\phi}{\partial n}\right|_{\mathrm{blade}} = 0 \tag{13}$$

Using Eq. (11), the continuity of pressure condition across the wake cut and the continuity of normal velocity condition are

$$\frac{\bar{\mathrm{D}}[[\phi]]}{\mathrm{D}t} = 0 \tag{14}$$

$$\left[\left[\frac{\partial\phi}{\partial n}\right]\right] = 0 \tag{15}$$

The downstream diffuser vanes are assumed to produce a potential disturbance that is harmonic in the tangential direction. Thus, the potential disturbance caused by the diffuser vanes at the outflow boundary is

$$\phi_i = e^{i\sigma\theta/G} \tag{16}$$

where the subscript i denotes the imposed disturbance and the magnitude of the harmonic disturbance is taken to be unity.

Unfortunately, this does not completely specify the outflow boundary condition because the imposed disturbance interacts with the impeller flow and scatters disturbances back through the outflow boundary. It also causes disturbances in the inviscid wake, which must be considered at the outflow boundary. The outflow boundary condition is, thus,

$$\phi_{\mathrm{outflow}} = \phi_i + \phi_o \tag{17}$$

where ϕ_o is an unknown potential defining the wake and backscattered disturbances.

The form of ϕ_o is obtained by solving the unsteady perturbation potential equation analytically in the vicinity of the outflow boundary. This is accomplished by assuming that the steady flow is constant and uniform, that is, ϕ_o is accurate only in small domains for which the actual steady flow does not vary by more than $\mathcal{O}(\varepsilon)$. Such a restriction causes slight inaccuracies because there may be steady flow gradients in the tangential direction at the outflow boundary. Thus, ϕ_o satisfies

$$\left(\frac{\bar{\mathrm{D}}^2}{\mathrm{D}t^2} - A^2\nabla^2\right)\Bigg|_{r=r_v}\phi_o = 0 \tag{18}$$

where r_v is the radius of the outflow boundary.

Because the perturbation potential may be discontinuous across the wake, ϕ_o is decomposed into a continuous part ϕ_c and a discontinuous part ϕ_d, that is, $\phi_o = \phi_c + \phi_d$. Both ϕ_c and ϕ_d must satisfy Eq. (18) as well as the wake boundary conditions.

Here ϕ_c is the general solution to Eq. (18). Unfortunately, there is no known closed-form solution, and so an approximate solution must be found. Because the imposed disturbance is harmonic in the tangential direction, so is ϕ_c. When the harmonic time dependence is included,

$$\tilde{\phi}_c = \bar{\phi}^m(r)\exp\left(ikt + ik_\theta^m\theta\right) \qquad m = 0, \pm1, \pm2, \ldots \quad (19)$$

where the tilde denotes the time dependence.

The periodicity requirement expressed in Eq. (8) dictates that k_θ^m be of the form

$$k_\theta^m = (\sigma + 2m\pi)/G \quad (20)$$

where $m = 0, \pm1, \pm2, \ldots$, is the unsteady disturbance mode number.

The form of $\bar{\phi}^m(r)$ is obtained by first transforming Eq. (18) to a coordinate system moving with the same tangential velocity as the steady flow at the outflow boundary. The new independent variables, denoted by tildes, are

$$\tilde{t} = t \qquad \tilde{\theta} = \theta - V_{\theta\,\mathrm{rel}}/r|_{r_v}t \qquad \tilde{r} = r \quad (21)$$

The transformed form of Eq. (18), including the harmonic time dependence, is

$$\left[\frac{1}{A^2}\frac{\partial^2}{\partial\tilde{t}^2} + 2M_r\frac{\partial^2}{\partial\tilde{r}\,\partial\tilde{t}} + \left(M_r^2 - 1\right)\frac{\partial^2}{\partial\tilde{r}^2} - \frac{1}{\tilde{r}}\frac{\partial}{\partial\tilde{r}} - \frac{1}{\tilde{r}^2}\frac{\partial^2}{\partial\tilde{\theta}^2}\right]_{r_v}\tilde{\phi}_c = 0 \quad (22)$$

where $M_r = V_r/A$.

The assumed solution [Eq. (19)] in transformed coordinates is

$$\tilde{\phi}_c = \bar{\phi}^m(r)\exp\left(i\bar{k}^m\tilde{t} + ik_\theta^m\tilde{\theta}\right) \qquad m = 0, \pm1, \pm2, \ldots \quad (23)$$

where $\bar{k}^m = k + k_\theta^m\left(V_{\theta\,\mathrm{rel}}/\tilde{r}\right)|_{r_v}$.

Substituting this into Eq. (22) leads to

$$\left\{\frac{\mathrm{d}^2}{\mathrm{d}\bar{r}^2} + \frac{1}{\Gamma^2}\left(\frac{1}{\bar{r}} - 2iM_r\right)\frac{\mathrm{d}}{\mathrm{d}\bar{r}} + \frac{1}{\Gamma^2}\left[1 - \left(\frac{k_\theta^m}{\bar{r}}\right)^2\right]\right\}_{r_v}\bar{\phi}^m = 0 \quad (24)$$

where $\bar{r} = \bar{k}^m\tilde{r}/A$ and $\Gamma^2 = 1 - M_r^2$.

If $M_r = 0$, Eq. (24) reduces to Bessel's equation, which has a well-known analytic solution. Unfortunately, M_r is not zero, and the equation has no known exact analytic solution. An approximate solution is obtained by first transforming the dependent variable such that the first derivative term goes to zero. The transformation is

$$\bar{\phi}^m(\bar{r}) = \hat{\phi}^m(\bar{r})\bar{r}^{-1/(2\Gamma^2)}\exp\left[i\left(M_r/\Gamma^2\right)\bar{r}\right] \quad (25)$$

Transforming Eq. (22) leads to

$$\left(\frac{\mathrm{d}^2}{\mathrm{d}\bar{r}^2} - f_m(\bar{r})\right)_{r_v}\hat{\phi}^m = 0 \quad (26)$$

where

$$f_m(\bar{r}) = -\frac{1}{\Gamma^2}\left[1 + \left(\frac{M_r}{\Gamma}\right)^2 - \frac{k_\theta^{m^2} - (2\Gamma^2 - 1)/(4\Gamma^2)}{\bar{r}^2} + i\frac{M_r}{\Gamma^2\bar{r}}\right]$$

One approximate solution to Eq. (26) is obtained by assuming $f_m(\bar{r})$ to be constant. A better approximation is made with the following Liouville–Green approximate solution (see Ref. 8), which is quite accurate if $f_m(\bar{r})$ varies slowly with $\bar{r}$:

$$\hat{\phi}^m(\bar{r}) = C_m^{\pm}f_m^{-\frac{1}{4}}(\bar{r})\exp\left[\pm\mathrm{sign}(\bar{r})\int f_m^{\frac{1}{2}}(\bar{r})\,\mathrm{d}\bar{r}\right] \quad (27)$$

where $C_m^{\pm}$ is an arbitrary constant. The sign is chosen so that the disturbance decays as it passes out of the domain.

Assuming the $f_m^{1/2}(\bar{r})$ term under the integral is constant and transforming back to the original coordinate system yields

$$\tilde{\phi}_c = C_m^{\pm}\hat{F}_m^{\pm}(\bar{r})\exp\left(ikt + ik_\theta^m\theta\right) \qquad m = 0, \pm1, \pm2, \ldots \quad (28)$$

where

$$\hat{F}_m^{\pm}(\bar{r}) = \bar{r}^{-1/(2\Gamma^2)}f_m^{-\frac{1}{4}}(\bar{r})\exp\left\{\left[i\left(M_r/\Gamma^2\right) \pm \mathrm{sign}(\bar{r})f_m^{\frac{1}{2}}(\bar{r})\right]\bar{r}\right\}$$

The perturbation potential describing continuous disturbances passing out the outflow boundary is

$$\phi_c = \sum_{m=-\infty}^{+\infty}C_m^-\hat{F}_m^-(\bar{r})\exp\left(ik_\theta^m\theta\right) \quad (29)$$

where harmonic time dependence is implicitly assumed.

Note that all of the waves decay exponentially because $f_m^{\frac{1}{2}}(\bar{r})$ has a nonzero real part. This is in contrast to the axial cascade case for which some of the waves propagate without decay as they pass out of the domain. Also, because ϕ_c is continuous, it automatically satisfies the wake boundary conditions.

The discontinuous part of the perturbation potential ϕ_d must satisfy the wake boundary conditions. The continuous pressure condition is satisfied by requiring that $[[\phi_d]]$ equal $[[\phi]]$ at some upstream location and also that ϕ_d satisfies the field equation $\bar{\mathrm{D}}\phi_d/\mathrm{D}t = 0$. Substituting this into Eq. (8) yields a second field equation for ϕ_d, that is, $\nabla^2|_{r=r_v}\phi_d = 0$. To solve these two field equations, ϕ_d is assumed to have the form

$$\phi_d = \bar{\phi}_d(r)\exp(i\lambda\theta) \quad (30)$$

where the two unknowns are the tangential wave number λ and the magnitude $\bar{\phi}_d(r)$.

When standard techniques are used, the solution is

$$\phi_d = W_1r^{\lambda^+}\exp(i\lambda^+\theta) + W_2r^{-\lambda^-}\exp(i\lambda^-\theta) \quad (31)$$

where $\lambda^{\pm} = -[ikr/(iV_\theta \pm V_r)]$. W_1 and W_2 are constants that are determined using the two wake boundary conditions after transforming to computational coordinates. Because $\lambda^{\pm}$ does not equal k_θ^m, the periodicity condition causes ϕ_d to be discontinuous across the wake.

The complete analytic expression for the perturbation potential in the vicinity of the outflow boundary is the sum of ϕ_i, ϕ_c, and ϕ_d:

$$\phi_{\mathrm{outflow}} = \exp\left(ik_\theta^m\theta\right) + \sum_{m=-\infty}^{+\infty}C_m^-\hat{F}_m^-(\bar{r})\exp\left(ik_\theta^m\theta\right) + \left[W_1r^{\lambda^+}\exp(i\lambda^+\theta) + W_2r^{\lambda^-}\exp(i\lambda^-\theta)\right] \quad (32)$$

The inflow boundary is treated analogously to the outflow boundary except that there is no imposed disturbance. Analytic solutions are found to the simplified perturbation potential equation (18), and these are applied at the inflow boundary. Because the inflow boundary cuts through the blade, the analytic solutions must satisfy the boundary condition that the perturbation velocity is tangent to the impeller blade. This condition is very difficult, if not impossible, to satisfy unless the blades are radially oriented at the inflow boundary. For radially oriented blades, the blade surface boundary condition, becomes $\lambda^{\pm}\partial\phi/\partial\theta|_{\mathrm{blade}} = 0$. The analytic inflow boundary solution is

$$\phi_{\mathrm{inflow}} = \sum_{m=0}^{+\infty}C_m^+\hat{F}_m^+(\bar{r})\cos\left(k_d^m\theta\right) \quad (33)$$

where the tangential wave number is $k_d^m = m\pi/G$, $m = 0, 1, 2, \ldots$.

Although these tangential wave numbers assure that the blade surface boundary condition is satisfied, they cause the solution to be discontinuous across the blade because of the periodic flow requirement. Physically, this means that unsteady vorticity is shed from an upstream portion of the blade, that is, an upstream portion of the blade is experiencing unsteady lift. The magnitude of this unsteady lift is such that the blade surface boundary condition is satisfied at the inflow boundary.

Numerical Solution Procedure

The perturbation potential equation and boundary conditions are approximated with finite differences, thereby reducing them to a block tridiagonal system of linear equations solved using a standard matrix inversion technique. The grid lines in the streamwise and tangential directions (Fig. 2) are equally spaced with $\Delta\theta = G/(j_{\max} - 1)$ and $\Delta r = (r_v - r_i)/(i_{\max} - 1)$. The streamwise grid lines are not necessarily along the flow streamlines, except for $j = 1$ and $j_{\max}$, which are along the impeller blade and wake streamlines. To facilitate the implementation of the numerical solution procedure, the perturbation potential equation, boundary conditions, and grid are transformed to a new coordinate system that has one axis coincident with the blade and wake streamline.

Results and Discussion

To demonstrate this unsteady flow model for impeller blade flow-induced vibration analysis, the GMA 404, an Allison Gas Turbine designed centrifugal compressor is used as a baseline, thereby providing a realistic baseline geometry and flow conditions. The baseline impeller geometric and aerodynamic parameters are shown in Table 1. Unless explicitly stated, all geometry and flow conditions correspond to those shown in Table 1. Only the impeller exit portion is considered, with the blade geometry in this region modified to satisfy the requirement that the blade is radially oriented at the computational domain inlet. With the interblade phase angle σ, this linear model is general enough to handle any ratio of impeller blade count to diffuser blade count.

The effects of changing the impeller backsweep angle, the number of diffuser vanes, the impeller–diffuser radial spacing, the mass flow rate, and the impeller rotational speed are considered. Each of these unsteady flow analyses are performed in two steps. First, the steady flowfield is calculated. Second, the steady flow parameters are input to predict the unsteady perturbation flowfield. The unsteady blade pressures are normalized by the unsteady pressure produced by the diffuser vanes at the outflow boundary, that is, the diffuser vane leading-edge radius. This means that the unsteady pressure throughout the domain is of order 1.

Backsweep Effects

Impeller blade geometries with backsweep angles of 0, 20, and 40 deg are considered (Fig. 3). The blade shapes are determined by fitting a quadratic curve from r_i where the blade is radially oriented to r_t where the backsweep angle is specified.

Table 1 Baseline parameters

Parameter[a]	Value
NB	30
NV	16
r_i, in.	4.16 – 0.106 m
r_t, in.	5.14 – 0.130 m
r_v, in.	5.65 – 0.144 m
Absolute stagnation pressure at inlet P_{oi}, psi	42.16 – 2.907 × 10^5 Pa
Absolute stagnation temperature at inlet T_{oi}, °R	728.17 – 404.54 k
Two-dimensional mass flow rate, (slug/s)/ft	0.520 – 24.9 (kg/s)/m
Impeller rotational speed, rpm	36,014.9

[a]Subscript i refers to computational domain inlet.

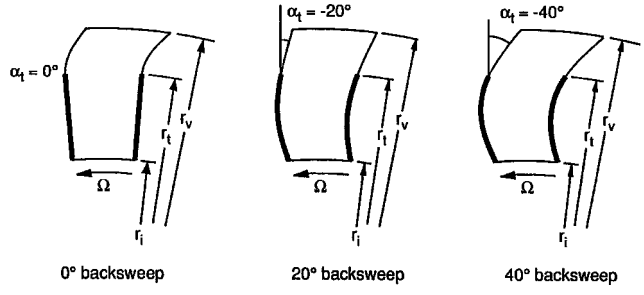

Fig. 3 Baseline impeller tip geometries with different backsweep angles.

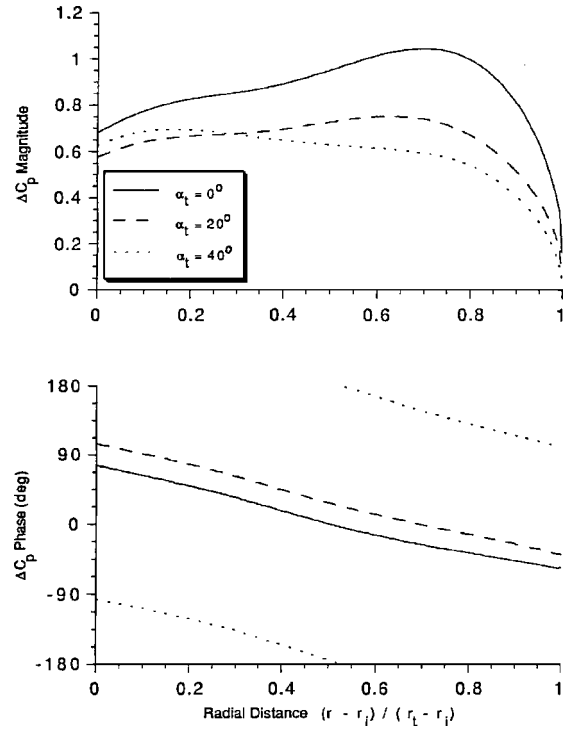

Fig. 4 Backsweep effect on unsteady pressure difference, one-dimensional steady flow.

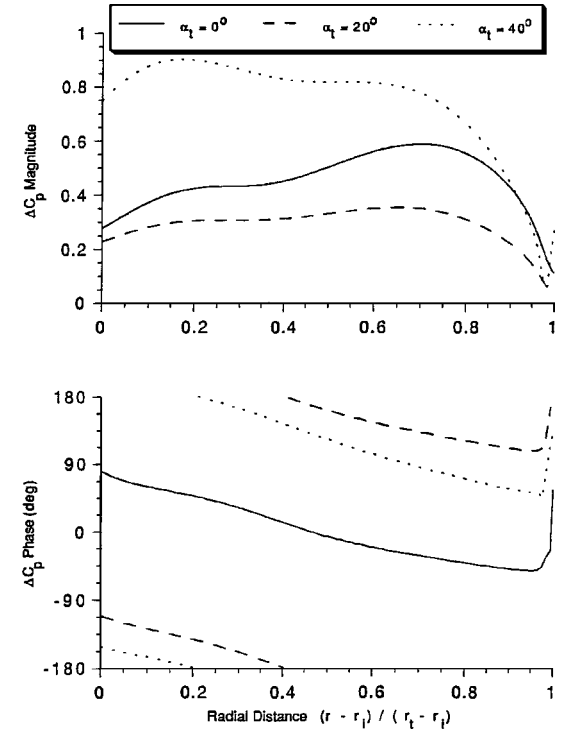

Fig. 5 Backsweep effect on unsteady pressure difference, two-dimensional steady flow.

With the one-dimensional steady flow (Fig. 4), the 0-deg backswept impeller has the largest unsteady pressure differential magnitude along the entire impeller blade, with the 40-deg backswept impeller having the smallest magnitude along the trailing 60% of the blade. The unsteady pressure differential phase changes very gradually along the blade for all three impellers. The phases of the 0- and 20-deg backswept impellers are similar, with the phase of the 40-deg backswept impeller having nearly a 180-deg shift.

With the two-dimensional steady flow (Fig. 5), the 40-deg backswept impeller has the largest unsteady pressure differential

Table 2 Impeller blade unsteady lift

	One-dimensional steady flow		Two-dimensional steady flow	
Parameter	Lift magnitude	Lift phase	Lift magnitude	Lift phase
Backsweep angle, deg				
0	0.13742	2.2500	0.07186	−3.7000
20	0.09797	33.100	0.04333	169.63
40	0.07735	−161.64	0.09773	139.34
Number of diffuser vanes				
11	0.12990	−72.300	0.03667	62.080
16	0.09797	33.100	0.04333	169.63
21	0.14649	147.28	0.07970	−70.810
Impeller–diffuser spacing (r_v/r_i)				
1.05	0.12409	−24.330	0.07720	−37.480
1.10	0.09797	33.100	0.04333	169.63
1.15	0.02608	101.61	0.11763	−167.28
Nondimensional mass flow rate				
0.149	0.10156	60.020	0.02736	−143.88
0.189	0.09797	33.100	0.04333	169.63
0.221	0.09526	15.610	0.04841	140.48
Impeller rotational speed, %				
90	0.02951	140.01	0.12390	69.110
95	0.05795	7.0500	0.12012	97.650
100	0.09797	32.100	0.04333	169.63

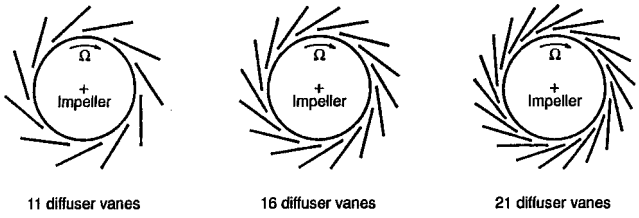

Fig. 6 Vaned diffuser configurations.

magnitude along most of the blade, the 20-deg backswept impeller has the smallest, with the 0-deg backswept impeller being in between. The unsteady pressure differential phase changes very gradually along the blade for all three impellers.

Table 2 presents the unsteady lift, determined by integrating the product of the unsteady pressure differential and cos(α) along the impeller blade. With the one-dimensional steady flow, the unsteady lift magnitude decreases as the backsweep angle increases. However, with the two-dimensional steady flow, the largest unsteady lift magnitude occurs for the largest backsweep angle. The unsteady lift magnitude obtained with the two-dimensional steady flow is much less than that obtained with the one-dimensional steady flow for the 0- and 20-deg backswept impellers. For the 40-deg backswept impeller, the unsteady lift magnitude is less with the one-dimensional steady flow. Thus, the one-dimensional steady flow results suggest that the impeller with a 40-deg backsweep yields the best design from a vibration point of view because for this case the unsteady lift magnitude is smallest. However, the results obtained with the two-dimensional steady flow suggest that the impeller with a 20-deg backsweep yields the lowest vibration design.

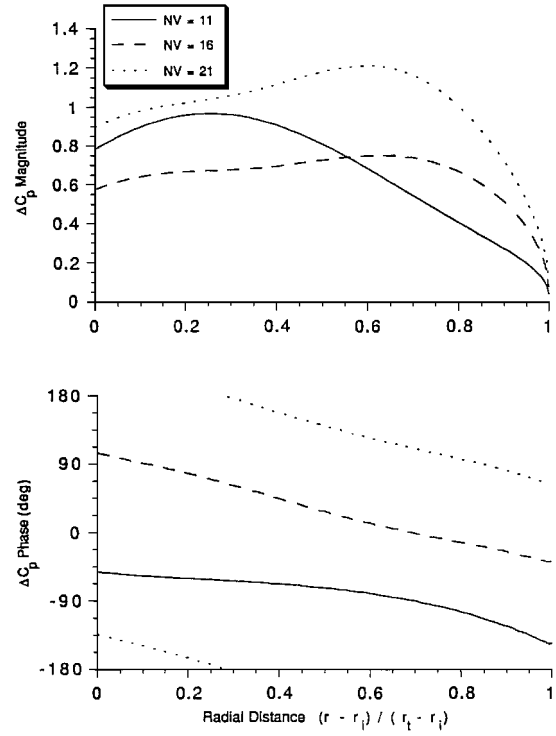

Fig. 7 Diffuser vane number effect on unsteady pressure difference, one-dimensional steady flow.

Number of Diffuser Vanes

Engine experience has shown that changing the number of diffuser vanes can significantly change the impeller blade unsteady pressure levels. To analyze this, the number of diffuser vanes is changed from 11 to 16 to 21 (Fig. 6).

With the one-dimensional steady flow (Fig. 7), the 21-vaned diffuser yields the largest unsteady pressure differential magnitude over the entire blade tip, with the 16-vaned diffuser yielding the smallest magnitude over the first half of the blade and the 11-vaned diffuser yielding the smallest magnitude over the second half of the blade. For the two-dimensional steady flow (Fig. 8), the unsteady pressure differential magnitude increases as the number of vanes increases. The unsteady pressure differential magnitude is larger with the one-dimensional steady flow. Both the one-dimensional and two-dimensional results show that the phase changes more rapidly along the blade as the number of diffuser vanes increases.

The unsteady lift for the two-dimensional flow is approximately half of that obtained with the one-dimensional steady flow (Table 2). The lowest vibration design with one-dimensional steady flow is the 16-vaned diffuser, whereas for the two-dimensional flow, the 11-vaned diffuser yields the lowest vibration design.

Impeller–Diffuser Spacing

When a designer is faced with an impeller aerodynamically forced vibration problem, increasing the radial spacing between the impeller and diffuser may be considered. In this model, changes in the impeller–diffuser spacing are made by changing the location of the exit of the grid relative to the impeller blades. The exit of the grid

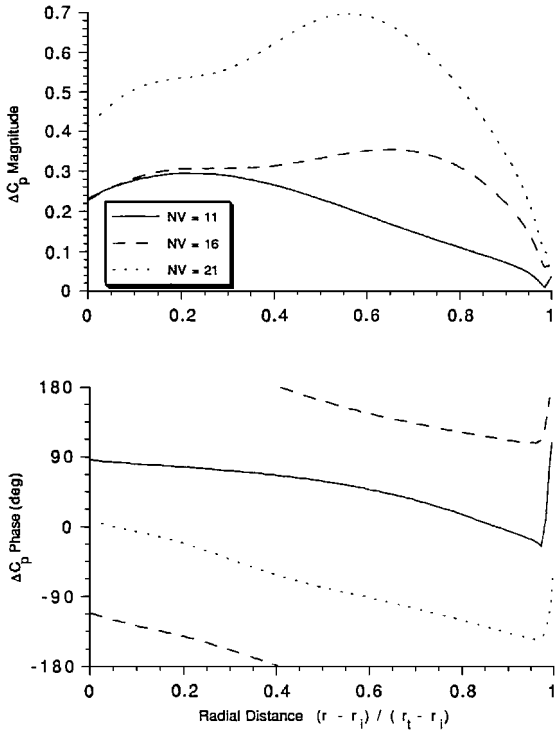

Fig. 8 Diffuser vane number effect on unsteady pressure difference, two-dimensional steady flow.

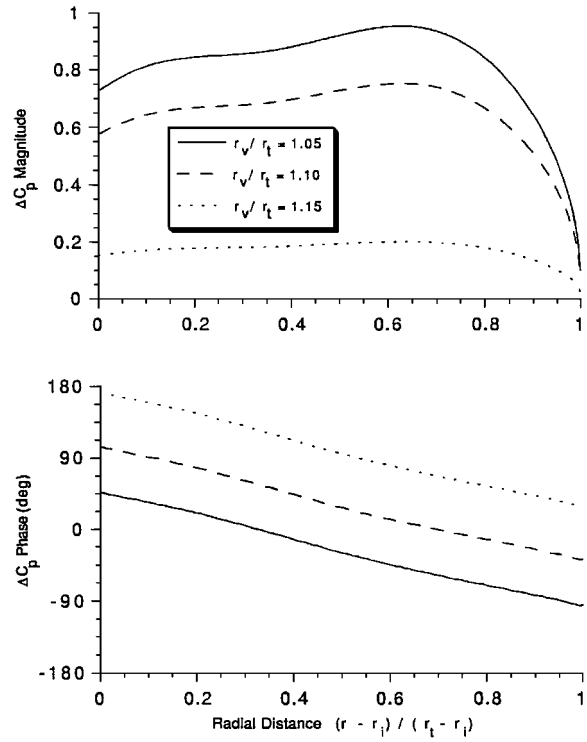

Fig. 10 Impeller–diffuser spacing effect on unsteady pressure difference, one-dimensional steady flow.

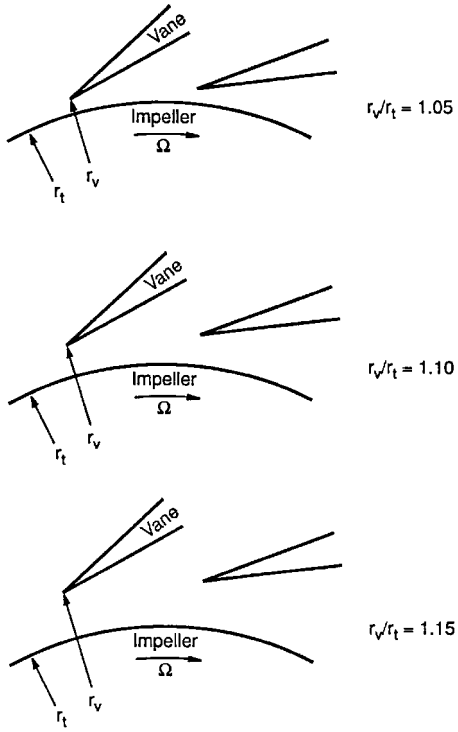

Fig. 9 Impeller–diffuser spacing variations.

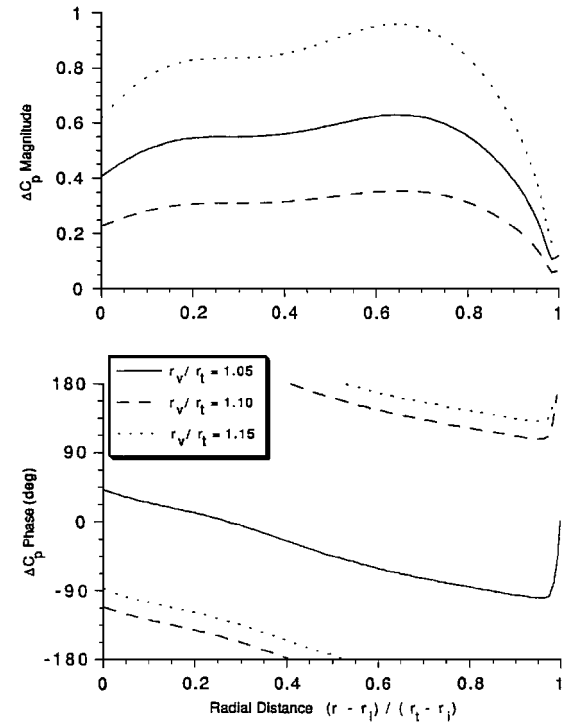

Fig. 11 Impeller–diffuser spacing effect on unsteady pressure difference, two-dimensional steady flow.

corresponds to the location of the leading edge of the diffuser vanes because the unsteady pressure potential disturbance generated by the vaned diffuser is imposed at the exit of the grid as part of the outflow boundary condition. The values of the ratio r_v/r_t considered are 1.05, 1.10, and 1.15 (Fig. 9). The baseline case corresponds to $r_v/r_t = 1.10$.

With one-dimensional steady flow (Fig. 10), the unsteady pressure differential magnitude decreases as the diffuser vanes are moved away from the impeller, with a relatively large decrease as the impeller–diffuser spacing ratio increases from 1.10 to 1.15. With two-dimensional steady flow (Fig. 11), the unsteady pressure differential magnitude decreases as the impeller–diffuser spacing ratio increases from 1.05 to 1.10. However, as the spacing ratio further increases to 1.15, the unsteady pressure differential magnitude increases to its largest value.

For the one-dimensional steady flow, the unsteady lift magnitude decreases as the impeller–diffuser spacing increases (Table 2). However, for the two-dimensional steady flow, the largest unsteady

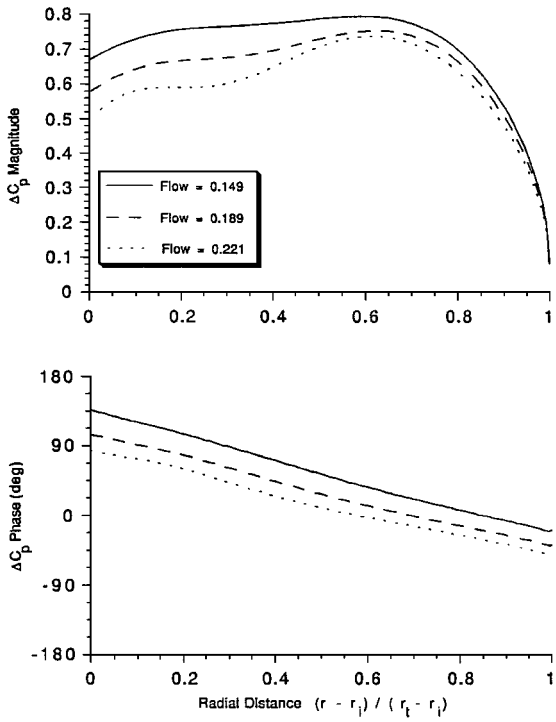

Fig. 12 Mass flow rate effect on unsteady pressure difference, one-dimensional steady flow.

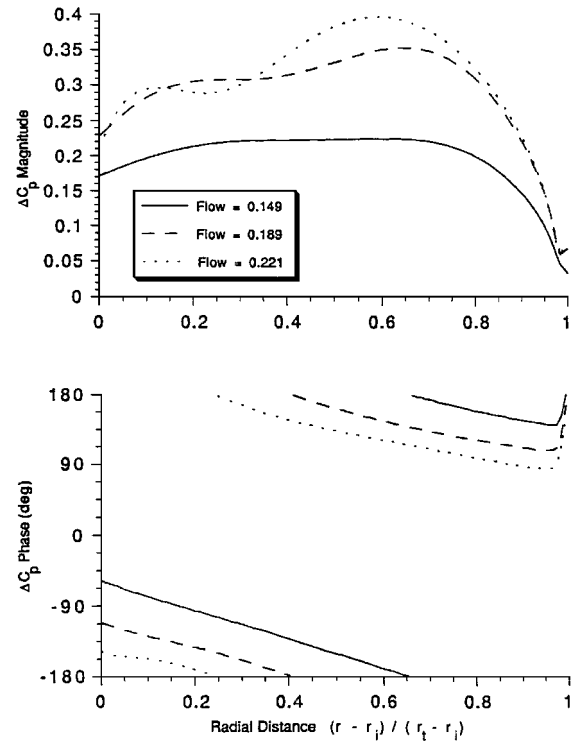

Fig. 13 Mass flow rate effect on unsteady pressure difference, two-dimensional steady flow.

lift occurs for the largest impeller–diffuser spacing, $r_v/r_t = 1.15$. With $r_v/r_t = 1.05$ and 1.10, the two-dimensional flow yields a much lower unsteady lift magnitude. The one-dimensional steady flow results suggest that the largest impeller–diffuser spacing, $r_v/r_t = 1.15$, yields the lowest vibration design, whereas the two-dimensional steady flow results suggest that $r_v/r_t = 1.10$ yields the lowest vibration design.

Mass Flow Rate

The mass flow rate is varied by changing the relative inlet velocity while all other aerodynamic parameters are kept at their baseline values. The nondimensional mass flow rates considered, 0.149, 0.189, and 0.221, correspond, respectively, to a mass-average value of M_r at the impeller tip of 0.199, 0.257, and 0.306.

With one-dimensional steady flow, as the mass flow rate decreases, the unsteady pressure differential magnitude increases (Fig. 12). The results obtained with the two-dimensional steady flow show the opposite trend, that is, as the mass flow rate decreases, the unsteady pressure differential magnitude decreases (Fig. 13). The unsteady pressure differential magnitudes obtained with two-dimensional steady flow are much lower than those obtained with one-dimensional steady flow.

For the one-dimensional steady flow, the unsteady lift magnitude decreases slightly as the mass flow rate is increased (Table 2). However, for the two-dimensional steady flow, the opposite trend is found, that is, the unsteady lift magnitude increases slightly as the mass flow rate is increased. For both the one-dimensional and two-dimensional steady flows, the mass flow rate has a relatively small effect on the unsteady lift magnitude. The one-dimensional steady flow results suggest the highest mass flow rate yields the lowest vibration design, whereas the two-dimensional steady flow results suggest the lowest mass flow rate yields the lowest vibration design.

Impeller Speed

There may also be vibration problems at intermediate points as the compressor increases its speed from idle. To simulate a change in compressor speed, more than one aerodynamic variable must be varied. Using aerodynamic design data for the Allison GMA 404 compressor, the mass flow rate, the impeller rotational speed, and

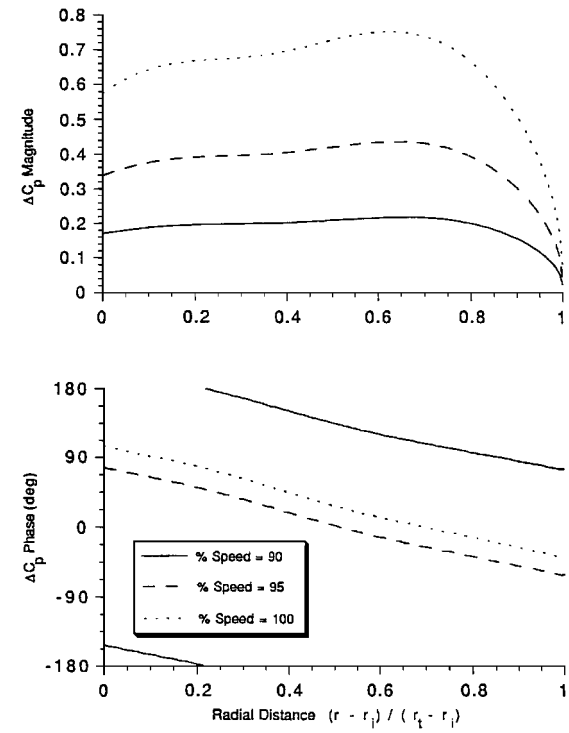

Fig. 14 Impeller speed effect on unsteady pressure difference, one-dimensional steady flow.

the total properties at the domain inlet are varied so as to simulate an increase in compressor speed.

With a one-dimensional steady flow (Fig. 14), the unsteady pressure differential magnitude increases as compressor speed increases. With two-dimensional steady flow (Fig. 15), the unsteady pressure differential magnitudes are nearly identical at the 90 and 95% speeds. At 100% speed, the magnitude drops to nearly a third of that obtained at 90 and 95% speeds.

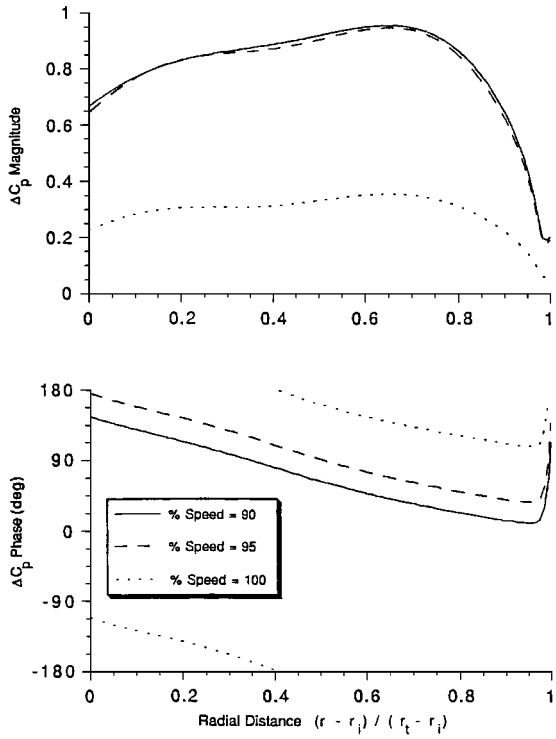

Fig. 15 Impeller speed effect on unsteady pressure difference, two-dimensional steady flow.

For one-dimensional steady flow, the unsteady lift magnitude decreases as the impeller speed increases (Table 2). However, with two-dimensional steady flow, the opposite trend is obtained: The unsteady lift magnitude increases as the impeller speed increases. The unsteady lift magnitude is much larger for the two-dimensional steady flow than for the one-dimensional flow for 90 and 95% speed. For the 100% speed case, the one-dimensional steady flow yields the larger unsteady lift magnitude.

Summary

To predict the unsteady aerodynamic response of impeller blades to the potential field generated by the downstream vaned diffuser, a small perturbation model of the unsteady flow in the outer radial portion of a centrifugal impeller has been developed. The model allows evaluation of the influence of several important geometric and aerodynamic parameters including the number of impeller blades and diffuser vanes, the impeller blade backsweep angle, the impeller rotational speed, and the mass flow rate.

To demonstrate the utility of the model, a series of studies were performed. Both two-dimensional and one-dimensional steady flow models were used for each study. The two-dimensional steady flow is consistent with the unsteady velocity potential equation because it is an irrotational flowfield. However, the one-dimensional steady flow is rotational and, thus, fundamentally inconsistent with the unsteady velocity potential equation. For this reason, the results obtained with the two-dimensional steady flow are considered more reliable.

Thus, this model can be used in determining what parameters to vary and by how much to diminish the amplitude of the aerodynamic forcing functions responsible for severe impeller vibration problems. The model can also be used in conjunction with experimental results to establish simplified guidelines for the designer regarding the suppression of impeller aerodynamically forced vibrations.

Acknowledgment

This research is sponsored, in part, by the GUIde Consortium on Bladed Disk Forced Response.

References

[1]Dring, R. P., Joslyn, H. D., Hardin, L. W., and Wagner, J. H., "Turbine Rotor-Stator Interaction," *American Society of Mechanical Engineers*, ASME Paper 82-GT-3, April 1982.

[2]Iino, T., and Kasai, K., "An Analysis of Unsteady Flow Induced by Interaction Between a Centrifugal Impeller and a Vaned Diffuser," *Transactions of the Japan Society of Mechanical Engineers*, Series B, Vol. 51, No. 471, 1985, pp. 154–159.

[3]Whitehead, D. S., "Force and Moment Coefficient for Vibrating Aerofoils in Cascade," Engineering Dept., Reports and Memoranda 3254, Cambridge Univ., Cambridge, England, U.K., Feb. 1960.

[4]Bryan, W. B., and Fleeter, S., "Flow-Induced Forced Response of an Incompressible Radial Cascade Including Profile and Incidence Effects," AIAA Paper 90-2352, 1990.

[5]Caruthers, J. E., and Kurosaka, M., "Flow Induced Vibration of Diffuser Excited Radial Compressors," NASA NAG 3-86, Sept. 1982.

[6]Verdon, J. M., "Linearized Unsteady Aerodynamic Theory," *AGARD Manual on Aeroelasticity in Axial Flow Turbomachines*, AGARD-AG-298, Vol. 1, 1987.

[7]McFarland, E. R., "A Rapid Blade-to-Blade Solution for Use in Turbomachinery Design," *Journal of Engineering for Power*, Vol. 106, No. 2, 1984, pp. 376–382.

[8]Olver, F. W. J., *Introduction to Asymptotics and Special Functions*, Chap. 6, Academic Press, New York, 1974, pp. 180–192.